



**HAL**  
open science

## Diffraction photoproduction of $j/\psi$ mesons with large momentum transfer at HERA

A. Aktas, V. Andreev, T. Anthonis, A. Astvatsatourov, A. Babaev, S. Backovic, J. Bahr, P. Baranov, E. Barrelet, W. Bartel, et al.

► **To cite this version:**

A. Aktas, V. Andreev, T. Anthonis, A. Astvatsatourov, A. Babaev, et al.. Diffraction photoproduction of  $j/\psi$  mesons with large momentum transfer at HERA. Physics Letters B, 2003, 568, pp.205-218. in2p3-00014098

**HAL Id: in2p3-00014098**

**<https://hal.in2p3.fr/in2p3-00014098>**

Submitted on 4 Nov 2003

**HAL** is a multi-disciplinary open access archive for the deposit and dissemination of scientific research documents, whether they are published or not. The documents may come from teaching and research institutions in France or abroad, or from public or private research centers.

L'archive ouverte pluridisciplinaire **HAL**, est destinée au dépôt et à la diffusion de documents scientifiques de niveau recherche, publiés ou non, émanant des établissements d'enseignement et de recherche français ou étrangers, des laboratoires publics ou privés.

# Diffractive Photoproduction of $J/\psi$ Mesons with Large Momentum Transfer at HERA

H1 Collaboration

## Abstract

The diffractive photoproduction of  $J/\psi$  mesons is measured with the H1 detector at the  $ep$  collider HERA using an integrated luminosity of  $78 \text{ pb}^{-1}$ . The differential cross section  $d\sigma(\gamma p \rightarrow J/\psi Y)/dt$  is studied in the range  $2 < |t| < 30 \text{ GeV}^2$ , where  $t$  is the square of the four-momentum transferred at the proton vertex. The cross section is also presented as a function of the photon-proton centre-of-mass energy  $W_{\gamma p}$  in three  $t$  intervals, spanning the range  $50 < W_{\gamma p} < 200 \text{ GeV}$ . A fast rise of the cross section with  $W_{\gamma p}$  is observed for each  $t$  range and the slope for the effective linear Pomeron trajectory is measured to be  $\alpha' = -0.0135 \pm 0.0074 \text{ (stat.)} \pm 0.0051 \text{ (syst.) GeV}^{-2}$ . The measurements are compared with perturbative QCD models based on BFKL and DGLAP evolution. The data are found to be compatible with  $s$ -channel helicity conservation.

Submitted to *Phys. Lett. B*.

A. Aktas<sup>10</sup>, V. Andreev<sup>24</sup>, T. Anthonis<sup>4</sup>, A. Astvatsatourov<sup>35</sup>, A. Babaev<sup>23</sup>, S. Backovic<sup>35</sup>,  
 J. Bähr<sup>35</sup>, P. Baranov<sup>24</sup>, E. Barrelet<sup>28</sup>, W. Bartel<sup>10</sup>, S. Baumgartner<sup>36</sup>, J. Becker<sup>37</sup>,  
 M. Beckingham<sup>21</sup>, A. Beglarian<sup>34</sup>, O. Behnke<sup>13</sup>, O. Behrendt<sup>7</sup>, A. Belousov<sup>24</sup>, Ch. Berger<sup>1</sup>,  
 T. Berndt<sup>14</sup>, J.C. Bizot<sup>26</sup>, J. Böhme<sup>10</sup>, M.-O. Boenig<sup>7</sup>, V. Boudry<sup>27</sup>, J. Bracinik<sup>25</sup>,  
 W. Braunschweig<sup>1</sup>, V. Brisson<sup>26</sup>, H.-B. Bröker<sup>2</sup>, D.P. Brown<sup>10</sup>, D. Bruncko<sup>16</sup>, F.W. Büsler<sup>11</sup>,  
 A. Bunyatyan<sup>12,34</sup>, A. Burrage<sup>18</sup>, G. Buschhorn<sup>25</sup>, L. Bystritskaya<sup>23</sup>, A.J. Campbell<sup>10</sup>,  
 S. Caron<sup>1</sup>, F. Cassol-Brunner<sup>22</sup>, V. Chekelian<sup>25</sup>, D. Clarke<sup>5</sup>, C. Collard<sup>4</sup>, J.G. Contreras<sup>7,41</sup>,  
 Y.R. Coppens<sup>3</sup>, J.A. Coughlan<sup>5</sup>, M.-C. Cousinou<sup>22</sup>, B.E. Cox<sup>21</sup>, G. Cozzika<sup>9</sup>, J. Cvach<sup>29</sup>,  
 J.B. Dainton<sup>18</sup>, W.D. Dau<sup>15</sup>, K. Daum<sup>33,39</sup>, M. Davidsson<sup>20</sup>, B. Delcourt<sup>26</sup>, N. Delerue<sup>22</sup>,  
 R. Demirchyan<sup>34</sup>, A. De Roeck<sup>10,43</sup>, E.A. De Wolf<sup>4</sup>, C. Diaconu<sup>22</sup>, J. Dingfelder<sup>13</sup>, P. Dixon<sup>19</sup>,  
 V. Dodonov<sup>12</sup>, J.D. Dowell<sup>3</sup>, A. Dubak<sup>25</sup>, C. Duprel<sup>2</sup>, G. Eckerlin<sup>10</sup>, V. Efremenko<sup>23</sup>, S. Egli<sup>32</sup>,  
 R. Eichler<sup>32</sup>, F. Eisele<sup>13</sup>, M. Ellerbrock<sup>13</sup>, E. Elsen<sup>10</sup>, M. Erdmann<sup>10,40,e</sup>, W. Erdmann<sup>36</sup>,  
 P.J.W. Faulkner<sup>3</sup>, L. Favart<sup>4</sup>, A. Fedotov<sup>23</sup>, R. Felst<sup>10</sup>, J. Ferencei<sup>10</sup>, S. Ferron<sup>27</sup>,  
 M. Fleischer<sup>10</sup>, P. Fleischmann<sup>10</sup>, Y.H. Fleming<sup>3</sup>, G. Flucke<sup>10</sup>, G. Flügge<sup>2</sup>, A. Fomenko<sup>24</sup>,  
 I. Foresti<sup>37</sup>, J. Formánek<sup>30</sup>, G. Franke<sup>10</sup>, G. Frising<sup>1</sup>, E. Gabathuler<sup>18</sup>, K. Gabathuler<sup>32</sup>,  
 J. Garvey<sup>3</sup>, J. Gassner<sup>32</sup>, J. Gayler<sup>10</sup>, R. Gerhards<sup>10</sup>, C. Gerlich<sup>13</sup>, S. Ghazaryan<sup>4,34</sup>,  
 L. Goerlich<sup>6</sup>, N. Gogitidze<sup>24</sup>, S. Gorbounov<sup>35</sup>, C. Grab<sup>36</sup>, V. Grabski<sup>34</sup>, H. Grässler<sup>2</sup>,  
 T. Greenshaw<sup>18</sup>, G. Grindhammer<sup>25</sup>, D. Haidt<sup>10</sup>, L. Hajduk<sup>6</sup>, J. Haller<sup>13</sup>, B. Heinemann<sup>18</sup>,  
 G. Heinzelmann<sup>11</sup>, R.C.W. Henderson<sup>17</sup>, H. Henschel<sup>35</sup>, O. Henshaw<sup>3</sup>, R. Heremans<sup>4</sup>,  
 G. Herrera<sup>7,44</sup>, I. Herynek<sup>29</sup>, M. Hildebrandt<sup>37</sup>, M. Hilgers<sup>36</sup>, K.H. Hiller<sup>35</sup>, J. Hladký<sup>29</sup>,  
 P. Höting<sup>2</sup>, D. Hoffmann<sup>22</sup>, R. Horisberger<sup>32</sup>, A. Hovhannisyan<sup>34</sup>, M. Ibbotson<sup>21</sup>,  
 M. Jacquet<sup>26</sup>, L. Janauschek<sup>25</sup>, X. Janssen<sup>4</sup>, V. Jemanov<sup>11</sup>, L. Jönsson<sup>20</sup>, C. Johnson<sup>3</sup>,  
 D.P. Johnson<sup>4</sup>, M.A.S. Jones<sup>18</sup>, H. Jung<sup>20,10</sup>, D. Kant<sup>19</sup>, M. Kapichine<sup>8</sup>, M. Karlsson<sup>20</sup>,  
 J. Katzy<sup>10</sup>, F. Keil<sup>14</sup>, N. Keller<sup>37</sup>, J. Kennedy<sup>18</sup>, I.R. Kenyon<sup>3</sup>, C. Kiesling<sup>25</sup>, M. Klein<sup>35</sup>,  
 C. Kleinwort<sup>10</sup>, T. Kluge<sup>1</sup>, G. Knies<sup>10</sup>, B. Koblitz<sup>25</sup>, S.D. Kolya<sup>21</sup>, V. Korbel<sup>10</sup>, P. Kostka<sup>35</sup>,  
 R. Koutouev<sup>12</sup>, A. Koutov<sup>8</sup>, J. Kroseberg<sup>37</sup>, K. Krüger<sup>10</sup>, J. Kueckens<sup>10</sup>, T. Kuhr<sup>10</sup>,  
 M.P.J. Landon<sup>19</sup>, W. Lange<sup>35</sup>, T. Laštovička<sup>35,30</sup>, P. Laycock<sup>18</sup>, A. Lebedev<sup>24</sup>, B. Leißner<sup>1</sup>,  
 R. Lemrani<sup>10</sup>, V. Lendermann<sup>10</sup>, S. Levonian<sup>10</sup>, B. List<sup>36</sup>, E. Lobodzinska<sup>10,6</sup>, N. Loktionova<sup>24</sup>,  
 R. Lopez-Fernandez<sup>10</sup>, V. Lubimov<sup>23</sup>, H. Lueders<sup>11</sup>, S. Lüders<sup>37</sup>, D. Lüke<sup>7,10</sup>, L. Lytkin<sup>12</sup>,  
 A. Makankine<sup>8</sup>, N. Malden<sup>21</sup>, E. Malinovski<sup>24</sup>, S. Mangano<sup>36</sup>, P. Marage<sup>4</sup>, J. Marks<sup>13</sup>,  
 R. Marshall<sup>21</sup>, H.-U. Martyn<sup>1</sup>, J. Martyniak<sup>6</sup>, S.J. Maxfield<sup>18</sup>, D. Meer<sup>36</sup>, A. Mehta<sup>18</sup>,  
 K. Meier<sup>14</sup>, A.B. Meyer<sup>11</sup>, H. Meyer<sup>33</sup>, J. Meyer<sup>10</sup>, S. Michine<sup>24</sup>, S. Mikocki<sup>6</sup>, D. Milstead<sup>18</sup>,  
 S. Mohrdieck<sup>11</sup>, F. Moreau<sup>27</sup>, A. Morozov<sup>8</sup>, J.V. Morris<sup>5</sup>, K. Müller<sup>37</sup>, P. Murín<sup>16,42</sup>,  
 V. Nagovizin<sup>23</sup>, B. Naroska<sup>11</sup>, J. Naumann<sup>7</sup>, Th. Naumann<sup>35</sup>, P.R. Newman<sup>3</sup>, F. Niebergall<sup>11</sup>,  
 C. Niebuhr<sup>10</sup>, D. Nikitin<sup>8</sup>, G. Nowak<sup>6</sup>, M. Nozicka<sup>30</sup>, B. Olivier<sup>10</sup>, J.E. Olsson<sup>10</sup>, D. Ozerov<sup>23</sup>,  
 V. Panassik<sup>8</sup>, C. Pascaud<sup>26</sup>, G.D. Patel<sup>18</sup>, M. Peez<sup>22</sup>, E. Perez<sup>9</sup>, A. Petrukhin<sup>35</sup>, J.P. Phillips<sup>18</sup>,  
 D. Pitzl<sup>10</sup>, R. Pöschl<sup>26</sup>, B. Povh<sup>12</sup>, N. Raicevic<sup>35</sup>, J. Rauschenberger<sup>11</sup>, P. Reimer<sup>29</sup>,  
 B. Reisert<sup>25</sup>, C. Risler<sup>25</sup>, E. Rizvi<sup>3</sup>, P. Robmann<sup>37</sup>, R. Roosen<sup>4</sup>, A. Rostovtsev<sup>23</sup>, S. Rusakov<sup>24</sup>,  
 K. Rybicki<sup>6,†</sup>, D.P.C. Sankey<sup>5</sup>, E. Sauvan<sup>22</sup>, S. Schätzel<sup>13</sup>, J. Scheins<sup>10</sup>, F.-P. Schilling<sup>10</sup>,  
 P. Schleper<sup>10</sup>, D. Schmidt<sup>33</sup>, S. Schmidt<sup>25</sup>, S. Schmitt<sup>37</sup>, M. Schneider<sup>22</sup>, L. Schoeffel<sup>9</sup>,  
 A. Schöning<sup>36</sup>, V. Schröder<sup>10</sup>, H.-C. Schultz-Coulon<sup>7</sup>, C. Schwanenberger<sup>10</sup>, K. Sedlák<sup>29</sup>,  
 F. Sefkow<sup>10</sup>, I. Sheviakov<sup>24</sup>, L.N. Shtarkov<sup>24</sup>, Y. Sirois<sup>27</sup>, T. Sloan<sup>17</sup>, P. Smirnov<sup>24</sup>,  
 Y. Soloviev<sup>24</sup>, D. South<sup>21</sup>, V. Spaskov<sup>8</sup>, A. Specka<sup>27</sup>, H. Spitzer<sup>11</sup>, R. Stamen<sup>10</sup>, B. Stella<sup>31</sup>,  
 J. Stiewe<sup>14</sup>, I. Strauch<sup>10</sup>, U. Straumann<sup>37</sup>, G. Thompson<sup>19</sup>, P.D. Thompson<sup>3</sup>, F. Tomasz<sup>14</sup>,  
 D. Traynor<sup>19</sup>, P. Truöl<sup>37</sup>, G. Tsipolitis<sup>10,38</sup>, I. Tsurin<sup>35</sup>, J. Turnau<sup>6</sup>, J.E. Turney<sup>19</sup>,  
 E. Tzamariudaki<sup>25</sup>, A. Uraev<sup>23</sup>, M. Urban<sup>37</sup>, A. Usik<sup>24</sup>, S. Valkár<sup>30</sup>, A. Valkárová<sup>30</sup>,

C. Vallée<sup>22</sup>, P. Van Mechelen<sup>4</sup>, A. Vargas Trevino<sup>7</sup>, S. Vassiliev<sup>8</sup>, Y. Vazdik<sup>24</sup>, C. Veelken<sup>18</sup>, A. Vest<sup>1</sup>, A. Vichnevski<sup>8</sup>, V. Volchinski<sup>34</sup>, K. Wacker<sup>7</sup>, J. Wagner<sup>10</sup>, R. Wallny<sup>37</sup>, B. Waugh<sup>21</sup>, G. Weber<sup>11</sup>, R. Weber<sup>36</sup>, D. Wegener<sup>7</sup>, C. Werner<sup>13</sup>, N. Werner<sup>37</sup>, M. Wessels<sup>1</sup>, B. Wessling<sup>11</sup>, M. Winde<sup>35</sup>, G.-G. Winter<sup>10</sup>, Ch. Wissing<sup>7</sup>, E.-E. Woehrling<sup>3</sup>, E. Wunsch<sup>10</sup>, A.C. Wyatt<sup>21</sup>, J. Žáček<sup>30</sup>, J. Zálešák<sup>30</sup>, Z. Zhang<sup>26</sup>, A. Zhokin<sup>23</sup>, F. Zomer<sup>26</sup>, and M. zur Nedden<sup>25</sup>

<sup>1</sup> *I. Physikalisches Institut der RWTH, Aachen, Germany<sup>a</sup>*

<sup>2</sup> *III. Physikalisches Institut der RWTH, Aachen, Germany<sup>a</sup>*

<sup>3</sup> *School of Physics and Space Research, University of Birmingham, Birmingham, UK<sup>b</sup>*

<sup>4</sup> *Inter-University Institute for High Energies ULB-VUB, Brussels; Universiteit Antwerpen (UIA), Antwerpen; Belgium<sup>c</sup>*

<sup>5</sup> *Rutherford Appleton Laboratory, Chilton, Didcot, UK<sup>b</sup>*

<sup>6</sup> *Institute for Nuclear Physics, Cracow, Poland<sup>d</sup>*

<sup>7</sup> *Institut für Physik, Universität Dortmund, Dortmund, Germany<sup>a</sup>*

<sup>8</sup> *Joint Institute for Nuclear Research, Dubna, Russia*

<sup>9</sup> *CEA, DSM/DAPNIA, CE-Saclay, Gif-sur-Yvette, France*

<sup>10</sup> *DESY, Hamburg, Germany*

<sup>11</sup> *Institut für Experimentalphysik, Universität Hamburg, Hamburg, Germany<sup>a</sup>*

<sup>12</sup> *Max-Planck-Institut für Kernphysik, Heidelberg, Germany*

<sup>13</sup> *Physikalisches Institut, Universität Heidelberg, Heidelberg, Germany<sup>a</sup>*

<sup>14</sup> *Kirchhoff-Institut für Physik, Universität Heidelberg, Heidelberg, Germany<sup>a</sup>*

<sup>15</sup> *Institut für experimentelle und Angewandte Physik, Universität Kiel, Kiel, Germany*

<sup>16</sup> *Institute of Experimental Physics, Slovak Academy of Sciences, Košice, Slovak Republic<sup>e,f</sup>*

<sup>17</sup> *School of Physics and Chemistry, University of Lancaster, Lancaster, UK<sup>b</sup>*

<sup>18</sup> *Department of Physics, University of Liverpool, Liverpool, UK<sup>b</sup>*

<sup>19</sup> *Queen Mary and Westfield College, London, UK<sup>b</sup>*

<sup>20</sup> *Physics Department, University of Lund, Lund, Sweden<sup>g</sup>*

<sup>21</sup> *Physics Department, University of Manchester, Manchester, UK<sup>b</sup>*

<sup>22</sup> *CPPM, CNRS/IN2P3 - Univ Mediterranee, Marseille - France*

<sup>23</sup> *Institute for Theoretical and Experimental Physics, Moscow, Russia<sup>l</sup>*

<sup>24</sup> *Lebedev Physical Institute, Moscow, Russia<sup>e</sup>*

<sup>25</sup> *Max-Planck-Institut für Physik, München, Germany*

<sup>26</sup> *LAL, Université de Paris-Sud, IN2P3-CNRS, Orsay, France*

<sup>27</sup> *LPNHE, Ecole Polytechnique, IN2P3-CNRS, Palaiseau, France*

<sup>28</sup> *LPNHE, Universités Paris VI and VII, IN2P3-CNRS, Paris, France*

<sup>29</sup> *Institute of Physics, Academy of Sciences of the Czech Republic, Praha, Czech Republic<sup>e,i</sup>*

<sup>30</sup> *Faculty of Mathematics and Physics, Charles University, Praha, Czech Republic<sup>e,i</sup>*

<sup>31</sup> *Dipartimento di Fisica Università di Roma Tre and INFN Roma 3, Roma, Italy*

<sup>32</sup> *Paul Scherrer Institut, Villigen, Switzerland*

<sup>33</sup> *Fachbereich Physik, Bergische Universität Gesamthochschule Wuppertal, Wuppertal, Germany*

<sup>34</sup> *Yerevan Physics Institute, Yerevan, Armenia*

<sup>35</sup> *DESY, Zeuthen, Germany*

<sup>36</sup> *Institut für Teilchenphysik, ETH, Zürich, Switzerland<sup>j</sup>*

<sup>37</sup> *Physik-Institut der Universität Zürich, Zürich, Switzerland<sup>j</sup>*

<sup>38</sup> Also at Physics Department, National Technical University, Zografou Campus, GR-15773 Athens, Greece

<sup>39</sup> Also at Rechenzentrum, Bergische Universität Gesamthochschule Wuppertal, Germany

<sup>40</sup> Also at Institut für Experimentelle Kernphysik, Universität Karlsruhe, Karlsruhe, Germany

<sup>41</sup> Also at Dept. Fis. Ap. CINVESTAV, Mérida, Yucatán, México<sup>k</sup>

<sup>42</sup> Also at University of P.J. Šafárik, Košice, Slovak Republic

<sup>43</sup> Also at CERN, Geneva, Switzerland

<sup>44</sup> Also at Dept. Fis. CINVESTAV, México City, México<sup>k</sup>

<sup>a</sup> Supported by the Bundesministerium für Bildung und Forschung, FRG, under contract numbers 05 H1 1GUA /1, 05 H1 1PAA /1, 05 H1 1PAB /9, 05 H1 1PEA /6, 05 H1 1VHA /7 and 05 H1 1VHB /5

<sup>b</sup> Supported by the UK Particle Physics and Astronomy Research Council, and formerly by the UK Science and Engineering Research Council

<sup>c</sup> Supported by FNRS-FWO-Vlaanderen, IISN-IKW and IWT

<sup>d</sup> Partially Supported by the Polish State Committee for Scientific Research, grant no. 2P0310318 and SPUB/DESY/P03/DZ-1/99 and by the German Bundesministerium für Bildung und Forschung

<sup>e</sup> Supported by the Deutsche Forschungsgemeinschaft

<sup>f</sup> Supported by VEGA SR grant no. 2/1169/2001

<sup>g</sup> Supported by the Swedish Natural Science Research Council

<sup>i</sup> Supported by the Ministry of Education of the Czech Republic under the projects INGO-LA116/2000 and LN00A006, by GAUK grant no 173/2000

<sup>j</sup> Supported by the Swiss National Science Foundation

<sup>k</sup> Supported by CONACyT

<sup>l</sup> Partially Supported by Russian Foundation for Basic Research, grant no. 00-15-96584

<sup>†</sup> Deceased

# 1 Introduction

The diffractive photoproduction of  $J/\psi$  mesons with large negative momentum transfer squared  $t$  at the proton vertex is a powerful means to probe the parton dynamics of the diffractive exchange. The variable  $t$  provides a relevant scale to investigate the application of perturbative QCD (pQCD). The diffractive photoproduction of vector mesons can be modelled in the proton rest frame, where the photon fluctuates into a  $q\bar{q}$  pair at a long distance from the proton target. The colour singlet exchange between the  $q\bar{q}$  fluctuation and the proton is realised in lowest order QCD by the exchange of a pair of gluons with opposite colour. In the leading logarithmic (LL) approximation, this process is described by the effective exchange of a gluonic ladder. At sufficiently low values of Bjorken  $x$  (i.e. large values of the centre-of-mass energy  $W_{\gamma p}$ ), the gluon ladder is expected to include contributions from BFKL evolution [1], as well as from standard DGLAP evolution [2]. Compared with other channels which have been used to search for BFKL evolution [3, 4, 8, 5, 6, 7], the measurement of diffractive  $J/\psi$  production at large  $|t|$  provides an experimentally clean signature in which the accurate measurement of the  $J/\psi$  four-momentum allows the kinematic dependences of the process to be determined precisely.

In this paper, an analysis of the diffractive photoproduction process  $\gamma p \rightarrow J/\psi Y$  is presented, extending into the hitherto unexplored region of large  $|t|$  ( $2 < |t| < 30 \text{ GeV}^2$ ). Here, the system  $Y$  represents either an elastically scattered proton or a dissociated proton system. For the range of  $|t|$  studied in this analysis, the contribution from elastic  $J/\psi$  production may be neglected due to its steep  $|t|$  dependence [9]. The cross section is measured differentially as a function of  $|t|$  and as a function of the photon-proton centre-of-mass energy  $W_{\gamma p}$  in different regions of  $|t|$ , using the  $J/\psi$  decay into two muons. To obtain information about the helicity structure of the interaction, the spin density matrix elements are extracted.

## 2 Perturbative QCD Models

Perturbative QCD models for the photoproduction of  $J/\psi$  mesons have been developed in the leading logarithmic approximation using either BFKL [10, 11, 12] or DGLAP [13] evolution. In the BFKL LL model the cross section depends linearly on the parton distribution of the proton and the gluon ladder couples to a single parton (dominantly a gluon) within the proton. The BFKL amplitude is expanded in terms of  $\log(x_h W_{\gamma p}^2 / W_0^2)$ , where  $x_h$  is the fraction of the proton momentum carried by the parton struck by the diffractive exchange. The scale parameter  $W_0$  is chosen to be half the vector meson mass  $M_V$ . The value of  $\alpha_s$  is fixed in the model to a value consistent with that extracted from a fit [12] to proton dissociative  $\rho$ ,  $\phi$  and  $J/\psi$  photoproduction data at HERA [14]. The BFKL LL model predicts an approximate power-law behaviour for the  $t$  dependence of the form  $d\sigma/dt \propto |t|^{-n}$ , where  $n$  is a function of  $|t|$ . For the kinematic range studied here,  $n$  increases from around 3 to 4 with increasing  $|t|$  and the approximation to a power-law improves as  $|t|$  increases. The calculation predicts a fast rise of the cross section  $\sigma \sim W_{\gamma p}^\delta$  with  $\delta \sim 1.4$ , which has little or no dependence on the value of  $t$ . In a recent paper [15], the LL calculations have been extended to incorporate the effects of higher conformal spin [16]. Although the full next-to-leading order terms of the BFKL amplitude have yet to be calculated for non-zero  $t$ , an estimate of the non-leading (NL) corrections was obtained

using kinematic constraints. In the DGLAP LL model, the cross section depends on the squared gluon distribution of the proton. The model predicts a non-exponential  $t$  dependence and a steep energy dependence which flattens as  $|t|$  approaches  $M_V^2$  due to the limited phase space available for evolution.

In the pQCD models [10, 11, 12, 13, 15], a non-relativistic approximation [17] for the  $J/\psi$  wavefunction is used in which the longitudinal momentum of the vector meson is shared equally between the quark and the anti-quark. In this approximation, the vector meson retains the helicity of the photon such that  $s$ -channel helicity conservation (SCHC) is satisfied [18].

### 3 Data Analysis

The data presented here were recorded in the years 1996 to 2000 and correspond to an integrated luminosity of  $78 \text{ pb}^{-1}$ . The majority of the data were collected when HERA was operated with positrons of energy 27.5 GeV and protons of 920 GeV. These data are combined with smaller data samples in which either the proton energy was 820 GeV or the positrons were replaced by electrons.

#### 3.1 The H1 Detector

A detailed description of the H1 detector can be found in [19] and only a short overview of the detector components most relevant to the present analysis is given here. The  $z$ -axis of the H1 detector is defined along the beam direction such that positive  $z$  values correspond to the direction of the outgoing proton beam.

Charged particles emerging from the interaction region are measured by the central tracking detector (CTD) in the pseudorapidity range  $-1.74 < \eta < 1.74$ <sup>1</sup>. The CTD comprises two large cylindrical central jet drift chambers (CJC) and two  $z$ -chambers arranged concentrically around the beam-line within a solenoidal magnetic field of 1.15 T. The CTD also provides triggering information based on track segments in the  $r - \phi$  plane from the CJC and the  $z$ -position of the vertex from a double layer of multi-wire proportional chambers. The energies of final state particles are measured in the liquid argon (LAr) calorimeter, which surrounds the tracking chambers and covers the range  $-1.5 < \eta < 3.4$ . The backward region ( $-4.0 < \eta < -1.4$ ) is covered by a lead-scintillating fibre calorimeter (SPACAL [20]) with electromagnetic and hadronic sections. The calorimeters are surrounded by the iron return yoke of the solenoidal magnet. The tracks of muons which penetrate the main detector are reconstructed from streamer tubes placed within the iron in the range  $-2.5 < \eta < 3.4$ . The luminosity is measured using the small angle Bremsstrahlung process ( $ep \rightarrow ep\gamma$ ) in which the final state photon is detected in a calorimeter, close to the beam-pipe, at 103 m from the nominal interaction point.

---

<sup>1</sup>The pseudorapidity  $\eta$  of an object detected with polar angle  $\theta$  is defined as  $\eta = -\ln \tan(\theta/2)$ .

## 3.2 Kinematics

The kinematics for diffractive charmonium production  $ep \rightarrow eJ/\psi Y$  are described in terms of the  $ep$  centre-of-mass-energy squared  $s = (k + p)^2$ , the virtuality of the photon  $Q^2 = -q^2 = -(k - k')^2$ , the square of the centre-of-mass energy of the initial photon-proton system  $W_{\gamma p}^2 = (q + p)^2$  and the four-momentum transfer squared  $t = (p - p_Y)^2$ . Here  $k$  ( $k'$ ) is the four-momentum of the incident (scattered) lepton and  $q$  is the four-momentum of the virtual photon. The four-momentum of the incident proton is denoted by  $p$  and  $p_Y$  is the four-momentum of the system  $Y$ . The event elasticity is defined as  $z = (p \cdot p_\psi)/(p \cdot q)$  where  $p_\psi$  is the four-momentum of the  $J/\psi$ . In the proton rest frame  $z$  is equal to the fractional energy of the photon transferred to the vector meson.

## 3.3 Event Selection

In this analysis, the  $J/\psi$  mesons are detected via their decay into two oppositely charged muons (branching fraction  $5.88 \pm 0.10\%$  [21]). The data were selected by a combination of triggers based on muon and track signatures. The selected events are required to have a vertex located in  $z$  within 40 cm of the nominal interaction point. Events with two tracks of opposite charge in the CJC, each associated with the event vertex and each with pseudo-rapidity  $|\eta| < 1.74$  and transverse momentum  $p_T > 0.8$  GeV are used to form  $J/\psi$  candidates. Both decay muons are identified in the instrumented iron or as minimum ionising particles in the LAr calorimeter.

Photoproduction events are selected by the absence of a scattered beam lepton candidate in the LAr or SPACAL calorimeters. The accepted photoproduction event sample covers the range  $Q^2 \lesssim 1$  GeV<sup>2</sup> with an average  $\langle Q^2 \rangle \sim 0.06$  GeV<sup>2</sup>, as determined from Monte Carlo simulations.

In order to select diffractive events, the analysis is restricted to the region of elasticity  $z > 0.95$ . For the range of  $t$  and  $W_{\gamma p}$  studied in this paper, the cut  $z > 0.95$  restricts the invariant mass of the system  $Y$  to be in the range  $M_Y \lesssim 30$  GeV, through the relation  $z \simeq 1 - (M_Y^2 - t)/W_{\gamma p}^2$ . The measurement of  $z$  is obtained from  $(E - p_z)_{J/\psi} / \sum(E - p_z)$  where  $\sum(E - p_z)$  is calculated from all detected particles in the calorimeters and the CJC including the decay products of the  $J/\psi$ . The variable  $W_{\gamma p}$  is reconstructed using  $W_{\gamma p}^2 = \sum(E - p_z) \cdot 2E_p$  where  $E_p$  is the energy of the incident proton beam. In the kinematic region studied, the variable  $t$  is well approximated by the negative transverse momentum squared of the vector meson, i.e.  $t \simeq -p_{t,J/\psi}^2$ .

## 3.4 Monte Carlo Simulation

Monte Carlo simulations are used to correct the data for the effects of resolution, acceptance and efficiency losses. Samples of events from signal and background processes are passed through a detailed simulation of the detector response, based on the GEANT program [22], and through the same reconstruction software as was used for the data.

The Monte Carlo generator used for the simulation of proton dissociative diffractive  $J/\psi$  production is HITVM [23], which generates events according to the BFKL model described in

[10, 11]. The events are generated using the GRV94-HO parton density functions [24] and the partonic system is fragmented according to the Lund string model implemented within the JETSET program [25]. The generated  $M_Y$  distribution in HITVM has an approximate exponential dependence  $d\sigma/dM_Y \sim e^{-0.1M_Y}$ . SCHC is assumed for the photon to vector meson transition.

The final sample of events contains background from resonant and non-resonant sources. The resonant background is produced indirectly through the decay of  $\psi(2S)$  mesons. This contribution is simulated using a Monte Carlo sample of  $\psi(2S)$  mesons generated using the DIFFVM Monte Carlo generator [26] according to the  $\psi(2S)$   $t$  distribution and cross section ratio to  $J/\psi$  production measured at lower values of  $|t|$  [9]. A contribution of 4% is observed with no significant  $t$  dependence. The main contribution to the non-resonant background is from the QED  $\gamma\gamma \rightarrow \mu\mu$  process, which is simulated using the LPAIR [27] Monte Carlo generator.

### 3.5 Signal Extraction

The invariant mass spectrum for all events in the range  $|t| > 2 \text{ GeV}^2$ ,  $50 < W_{\gamma p} < 150 \text{ GeV}$  and  $z > 0.95$  is shown in figure 1. The LPAIR non-resonant background is normalised to the data in the side-bands outside the mass regions of the  $J/\psi$  and  $\psi(2S)$  resonances. The number of signal events is determined from the number of events in the mass window of  $2.9 < M_{\mu^+\mu^-} < 3.3 \text{ GeV}$ , after subtracting the contributions of the resonant and non-resonant backgrounds. The resulting number of  $J/\psi$  candidate events for the total sample shown in figure 1 is  $846 \pm 30$  (stat.).

### 3.6 Comparison of Data and Simulation

The HITVM model gives a reasonable description of the data which is further improved through small adjustments to the  $W_{\gamma p}$  and  $t$  distributions. After these adjustments a comparison between the simulation and the data, before background subtraction, is given in figure 2 for the region  $|t| > 2 \text{ GeV}^2$ ,  $50 < W_{\gamma p} < 150 \text{ GeV}$ ,  $z > 0.95$  and  $2.9 < M_{\mu^+\mu^-} < 3.3 \text{ GeV}$ . Distributions are shown for the polar angle and transverse momentum of the decay muon tracks, for the reconstructed value of the elasticity  $z$  (where the cut on  $z$  is not applied), for  $W_{\gamma p}$ , for the decay angular distributions  $\cos\theta^*$  and  $\phi^*$  (see section 4.2) and for the squared transverse momentum of the dimuon system  $p_{t,\mu^+\mu^-}^2$ . The structure in the  $\phi^*$  distribution (figure 2f) is due to the low acceptance for one of the muons, which has a low transverse momentum in the laboratory frame, when the  $J/\psi$  meson production and decay planes coincide ( $\phi^* \sim 0^\circ$  or  $\phi^* \sim \pm 180^\circ$ ).

### 3.7 Systematic Uncertainties

The uncertainties in detector effects and in the modelling of the underlying physics processes contribute to the systematic uncertainties in the cross section measurements. The following sources of systematic error are taken into account.

- The uncertainty in the acceptance corrections is estimated by reweighting the  $W_{\gamma p}$  distribution by  $W_{\gamma p}^{\pm 0.35}$  and the  $t$  distribution by  $t^{\pm 0.85}$ . The resulting systematic uncertainties on the cross section measurements range from 1% to 5%.
- The uncertainty in the mass distribution of the proton dissociative system  $Y$  is estimated by reweighting the  $M_Y$  dependence in HITVM by  $e^{\pm 0.06 M_Y}$ . This results in a variation of the cross section of about 4%, increasing up to 19% at the largest  $W_{\gamma p}$  and  $|t|$ .
- The effect of possible deviations from SCHC is estimated by modifying the simulated  $\cos \theta^*$  distribution. The cross sections alter by 5% on average.
- The uncertainty on the trigger efficiency, obtained from an independently triggered sample of events, gives a contribution to the systematic error of 6%.
- The uncertainty in the identification efficiency of muons is estimated by detailed comparison of the data and simulation efficiencies for an independent data sample. The resulting systematic uncertainty is 6%.
- The uncertainty due to the reconstruction efficiency of the central tracker for the two tracks leads to an error of 4%.
- The uncertainty in the non-resonant background subtraction is estimated by using a data side-band subtraction as an alternative to the Monte Carlo subtraction. A difference of  $\sim 2\%$  is found between the two methods and assigned to the systematic error.
- The uncertainty in the subtraction of the  $\psi(2S)$  background leads to an error of 2%, obtained by varying the normalisation and exponential  $t$  slope of the  $\psi(2S)$  cross section in the simulation.
- Other sources of systematic error are the uncertainty in the hadronic energy scale of the liquid argon calorimeter, the uncertainty in the luminosity measurement and the uncertainty in the branching fraction for the measured decay channel [21]. Each of them is responsible for an error of no more than 1.7%.

The total systematic error for each data point has been obtained by adding all individual contributions in quadrature. It has a small dependence on  $t$  with an average value of 12% and increases from around 11% at low  $W_{\gamma p}$  to 20% at high  $W_{\gamma p}$ . The part of the uncertainty which is uncorrelated between different data points contributes 8.5% to the systematic error. The statistical error is larger than the systematic error in the region  $|t| \geq 5.5 \text{ GeV}^2$ .

## 4 Results

### 4.1 Cross Sections

The differential cross section  $d\sigma/dt$  for the process  $ep \rightarrow eJ/\psi Y$  is obtained from the number of data events in each measurement interval after corrections for backgrounds and detector

effects, divided by the integrated luminosity, the branching fraction and the width of the interval. The cross section for the photoproduction process  $\gamma p \rightarrow J/\psi Y$  is obtained by dividing the differential  $ep$  cross section by the effective photon flux [28] integrated over the  $W_{\gamma p}$  and  $Q^2$  ranges of the measurement. QED radiative effects are estimated to be less than 1% and are neglected. The differential photoproduction cross section  $d\sigma/dt$  is shown in figure 3 and table 1 for the kinematic region  $50 < W_{\gamma p} < 150$  GeV and  $z > 0.95$ . The data are plotted at the mean value in each  $t$  interval according to a parameterisation of the data. In the region  $|t| > 3.45$  GeV<sup>2</sup>, the data in figure 3 are adequately described by a power-law dependence of the form  $A \cdot |t|^{-n}$  where  $n = 3.00 \pm 0.08$  (stat.)  $\pm 0.05$  (syst.). When the power-law fit is repeated, each time increasing the starting value of  $|t|$  in the fit, the value of  $n$  is found to increase systematically up to a value of  $n = 3.78 \pm 0.17$  (stat.)  $\pm 0.06$  (syst.) for  $|t| > 10.4$  GeV<sup>2</sup>. The data are incompatible with an exponential behaviour  $d\sigma/dt \propto e^{bt}$  which was found to give a reasonable description of the proton dissociative  $J/\psi$  cross section at lower values of  $|t|$  ( $|t| < 5$  GeV<sup>2</sup>) [9].

In figure 3 the data are compared with the predictions from pQCD calculations in the BFKL leading logarithmic approximation [15] (solid curve), including non-leading corrections with fixed  $\alpha_s$  [15] (dashed curve) and including non-leading corrections with running  $\alpha_s$  [15] (dotted curve). The  $t$  dependence and normalisation of the data are well described by the BFKL LL approximation when the parameters of the model are set to values consistent with those extracted from a fit [12] to various vector meson proton dissociation data at HERA covering a smaller  $|t|$  range [14], i.e. the scale parameter is set to  $W_0 = M_V/2$  and  $\alpha_s$  is fixed at 0.18. The normalisation uncertainty due to the choice of  $W_0$  is large. For example, using  $W_0 = M_V/4$  ( $W_0 = M_V$ ) leads to an increase (decrease) in the normalisation of the prediction by a factor of approximately two. The inclusion of NL corrections with a fixed strong coupling  $\alpha_s$  leads to only a small difference with respect to the LL prediction. However, with a running  $\alpha_s$  the  $t$  dependence becomes steeper and the prediction is unable to describe the data across the whole  $t$  range. The uncertainties in the choice of the scale parameter, proton parton density and other parameters used in the NL calculation have only a small effect on the shape of the predictions in comparison to the treatment of  $\alpha_s$ . The data are also compared with calculations in the DGLAP LL approximation [13] (dashed-dotted curve) in the region of validity for the model  $|t| < M_{J/\psi}^2$ . The data are well described in shape and normalisation when the separation parameter  $t_0$ , which represents the value of  $t$  at which the prediction for proton dissociation matches the elastic cross section, is set to  $-0.60$  GeV<sup>2</sup>.

The ZEUS collaboration has recently published data on the diffractive production of  $J/\psi$  mesons with proton dissociation in the range  $1.2 < |t| < 6.5$  GeV<sup>2</sup>,  $80 < W_{\gamma p} < 120$  GeV and  $x_h = |t|/(W_{\gamma p}^2(1-z)) > 0.01$  [14]. When the present analysis is performed in this kinematic region, good agreement between the H1 and ZEUS results is observed.

In figure 4 and tables 2 - 4, the cross section  $\sigma_{\gamma p \rightarrow J/\psi Y}$  is presented as a function of  $W_{\gamma p}$  for three ranges of  $t$  in the kinematic region  $z > 0.95$ . The data in each  $t$  range are consistent with a power-law dependence of the form  $\sigma \propto W_{\gamma p}^\delta$  and the results of power-law fits for  $\delta$  are given in table 5. The contribution from correlated systematic errors is calculated by shifting the data points according to each source of uncertainty and repeating the fits. The values of the power  $\delta$  in each  $t$  range are similar to the results from the proton elastic process for  $J/\psi$  mesons at low  $|t|$  measured over a similar range of  $W_{\gamma p}$  [29]. In a Regge pole model, the power-law

dependence can be expressed as  $d\sigma/dt = F(t)W_{\gamma p}^{4\alpha(t)-4}$  where  $F(t)$  is a function of  $t$  only. The value of  $\alpha(t)$  at each  $t$  value is obtained from  $\alpha = (\delta + 4)/4$  and is also shown in table 5. Assuming a single effective Pomeron trajectory of the linear form  $\alpha(t) = \alpha(0) + \alpha't$ , a fit to the three  $\alpha$  values yields a slope of  $\alpha' = -0.0135 \pm 0.0074$  (stat.)  $\pm 0.0051$  (syst.)  $\text{GeV}^{-2}$  with an intercept of  $\alpha(0) = 1.167 \pm 0.048$  (stat.)  $\pm 0.024$  (syst.). The value of the slope parameter  $\alpha'$  is lower than that observed for the elastic photoproduction of  $J/\psi$  mesons at low  $|t|$  [30]. It is also significantly different from observations at low  $|t|$  in hadron-hadron scattering, where a value of  $\alpha' = 0.26 \pm 0.02 \text{ GeV}^{-2}$  [31] was obtained.

In figure 4 the data are compared with the BFKL theoretical predictions for the LL approximation (solid curve) and the LL+NL prediction with fixed  $\alpha_s$  (dashed curve). The data are also compared with the DGLAP LL predictions (dashed-dotted curve). The BFKL LL contribution gives a reasonable description of the energy dependence, except for the lowest  $|t|$  range where it is steeper than the data. The BFKL LL+NL prediction with fixed  $\alpha_s$  is similar to that of the BFKL LL prediction. The DGLAP LL model, which is valid in the range  $|t| < M_{J/\psi}^2$ , describes the energy dependence in the lowest  $|t|$  range,  $2 < |t| < 5 \text{ GeV}^2$ . In the region  $5 < |t| < 10 \text{ GeV}^2$ , where  $|t|$  approaches  $M_{J/\psi}^2$ , the description becomes worse.

## 4.2 Spin Density Matrix Elements

The polar ( $\theta^*$ ) and azimuthal ( $\phi^*$ ) decay angular distributions are measured in the rest frame of the  $J/\psi$  with the quantisation axis taken as the direction of the meson in the photon-proton centre-of-mass frame (helicity frame). The normalised two-dimensional angular distribution for the decay of the  $J/\psi$  meson to fermions is written in terms of spin density matrix elements  $r_{00}^{04}$ ,  $r_{1-1}^{04}$  and  $\text{Re}\{r_{10}^{04}\}$  [32] as

$$\frac{1}{\sigma} \frac{d^2\sigma}{d\cos\theta^* d\phi^*} = \frac{3}{4\pi} \left( \frac{1}{2}(1 + r_{00}^{04}) - \frac{1}{2}(3r_{00}^{04} - 1) \cos^2\theta^* \right. \\ \left. + \sqrt{2}\text{Re}\{r_{10}^{04}\} \sin 2\theta^* \cos\phi^* + r_{1-1}^{04} \sin^2\theta^* \cos 2\phi^* \right). \quad (1)$$

The one-dimensional distributions are obtained by integrating over  $\cos\theta^*$  or  $\phi^*$  and give  $\frac{d\sigma}{d\cos\theta^*} \propto 1 + r_{00}^{04} + (1 - 3r_{00}^{04}) \cos^2\theta^*$  and  $\frac{d\sigma}{d\phi^*} \propto 1 + r_{1-1}^{04} \cos 2\phi^*$ . Under the assumption of  $s$ -channel helicity conservation (SCHC), the  $J/\psi$  meson in photoproduction is expected to be fully transversely polarised and the matrix elements  $r_{00}^{04}$ ,  $r_{1-1}^{04}$  and  $\text{Re}\{r_{10}^{04}\}$  are zero.

The spin density matrix elements are extracted by a two-dimensional log likelihood fit of the data to equation (1). The normalised single differential distributions in  $\cos\theta^*$  and  $\phi^*$  are shown in figure 5 for three ranges of  $t$ . The dashed curve on the figure shows the expectation from SCHC and the solid curves show the results of the two-dimensional fit. The values of the three extracted matrix elements are shown in figure 6 and table 6 as a function of  $|t|$ . Measurements from the ZEUS collaboration of the spin density matrix elements for the photoproduction of  $\rho^0$  and  $J/\psi$  mesons [14] are also shown in the figure. In contrast to the  $\rho^0$  meson, the measured spin density matrix elements of the  $J/\psi$  meson are all compatible with zero, within experimental errors, and are thus compatible with SCHC. The  $J/\psi$  results are therefore consistent with the longitudinal momentum of the photon being shared symmetrically between the heavy quarks. Hence, the approximations made in the pQCD models [10, 11, 12, 13, 15] for the  $J/\psi$  wavefunction are satisfactory for the present data.

## 5 Summary

The differential cross section  $d\sigma/dt$  for the diffractive photoproduction of  $J/\psi$  mesons has been measured as a function of the momentum transfer squared  $t$  from  $|t| = 2 \text{ GeV}^2$  up to values as large as  $|t| = 30 \text{ GeV}^2$  in the kinematic region  $z > 0.95$  and  $50 < W_{\gamma p} < 150 \text{ GeV}$ . The data are well described in this region by pQCD calculations [15] using the leading logarithmic BFKL equation with parameters consistent with a fit to vector meson proton dissociation data at HERA [14]. The addition of non-leading corrections preserves the description of the data if the strong coupling  $\alpha_s$  is held fixed. The data in the region  $|t| < M_{J/\psi}^2$  are well described by a model [13] based on DGLAP evolution.

The cross section has also been measured as a function of  $W_{\gamma p}$  in three  $t$  intervals. The energy dependence shows a similar steep rise to that observed for elastic  $J/\psi$  production at low  $|t|$  [29] and the rise persists to the largest  $|t|$  values studied. The energy dependence is reasonably described by the BFKL model with the chosen parameters, except for the lowest  $|t|$  range ( $|t| < 5 \text{ GeV}^2$ ). The DGLAP model describes the energy dependence in the range  $|t| < 5 \text{ GeV}^2$ .

The measurement of the effective Pomeron trajectory at large  $|t|$  yields a slope of  $\alpha' = -0.0135 \pm 0.0074(\text{stat.}) \pm 0.0051(\text{syst.}) \text{ GeV}^{-2}$ . This is lower than that observed for elastic  $J/\psi$  photoproduction at low  $|t|$  [30] and also lower than the slope obtained from hadronic scattering ( $\alpha' = 0.26 \pm 0.02 \text{ GeV}^{-2}$  [31]). The observation of the effective slope being small is compatible with the predictions of models based on BFKL evolution [11].

The spin density matrix elements of the  $J/\psi$  have been extracted in three regions of  $t$ . The results are found to be consistent with  $s$ -channel helicity conservation within the experimental uncertainties and, therefore, are compatible with models [10, 11, 12, 13, 15] in which the longitudinal momentum of the photon is shared symmetrically between the quarks of the  $J/\psi$ .

## Acknowledgements

We are grateful to the HERA machine group whose outstanding efforts have made and continue to make this experiment possible. We thank the engineers and technicians for their work in constructing and maintaining the H1 detector, our funding agencies for financial support, the DESY technical staff for continual assistance and the DESY directorate for support and for the hospitality which they extend to the non-DESY members of the collaboration. We are grateful to R. Enberg, J. R. Forshaw, L. Motyka, G. Poludniowski, E. Gotsman, E. Levin, U. Maor and E. Naftali for providing us with the results of their models and for productive discussions.

## References

- [1] E. A. Kuraev, L. N. Lipatov and V. S. Fadin, Sov. Phys. JETP **44** (1976) 443 [Zh. Eksp. Teor. Fiz. **71** (1976) 840];  
E. A. Kuraev, L. N. Lipatov and V. S. Fadin, Sov. Phys. JETP **45** (1977) 199 [Zh. Eksp. Teor. Fiz. **72** (1977) 377];  
I. I. Balitsky and L. N. Lipatov, Sov. J. Nucl. Phys. **28** (1978) 822 [Yad. Fiz. **28** (1978) 1597].
- [2] V. N. Gribov and L. N. Lipatov, Yad. Fiz. **15** (1972) 781 and 1218 [Sov. J. Nucl. Phys. **15** (1972) 438 and 675];  
Y. L. Dokshitzer, Sov. Phys. JETP **46** (1977) 641 [Zh. Eksp. Teor. Fiz. **73** (1977) 1216];  
G. Altarelli and G. Parisi, Nucl. Phys. B **126** (1977) 298.
- [3] C. Adloff *et al.* [H1 Collaboration], Nucl. Phys. B **538** (1999) 3 [hep-ex/9809028].
- [4] C. Adloff *et al.* [H1 Collaboration], Phys. Lett. B **462** (1999) 440 [hep-ex/9907030].
- [5] M. Derrick *et al.* [ZEUS Collaboration], Phys. Lett. B **369** (1996) 55 [hep-ex/9510012].
- [6] R. Enberg, G. Ingelman and L. Motyka, Phys. Lett. B **524** (2002) 273 [hep-ph/0111090].
- [7] B. Cox, J. Forshaw and L. Lönnblad, JHEP **9910** (1999) 023 [hep-ph/9908464].
- [8] C. Adloff *et al.* [H1 Collaboration], Eur. Phys. J. C **24** (2002) 517 [hep-ex/0203011].
- [9] C. Adloff *et al.* [H1 Collaboration], Phys. Lett. B **541** (2002) 251 [hep-ex/0205107].
- [10] J. R. Forshaw and M. G. Ryskin, Z. Phys. C **68** (1995) 137 [hep-ph/9501376].
- [11] J. Bartels, J. R. Forshaw, H. Lotter and M. Wüsthoff, Phys. Lett. B **375** (1996) 301 [hep-ph/9601201].
- [12] J. R. Forshaw and G. Poludniowski, Eur. Phys. J. C **26** (2003) 411 [hep-ph/0107068].
- [13] E. Gotsman, E. Levin, U. Maor and E. Naftali, Phys. Lett. B **532** (2002) 37 [hep-ph/0110256].
- [14] S. Chekanov *et al.* [ZEUS Collaboration], Eur. Phys. J. C **26** (2003) 389 [hep-ex/0205081].
- [15] R. Enberg, L. Motyka and G. Poludniowski, Eur. Phys. J. C **26** (2002) 219 [hep-ph/0207027].
- [16] L. Motyka, A. D. Martin and M. G. Ryskin, Phys. Lett. B **524** (2002) 107 [hep-ph/0110273].
- [17] M. G. Ryskin, Z. Phys. C **57** (1993) 89.
- [18] E. V. Kuraev, N. N. Nikolaev and B. G. Zakharov, JETP Lett. **68** (1998) 696 [Pisma Zh. Eksp. Teor. Fiz. **68** (1998) 667] [hep-ph/9809539].
- [19] I. Abt *et al.* [H1 Collaboration], Nucl. Instrum. Meth. A **386** (1997) 310 and 348.

- [20] T. Nicholls *et al.* [H1 SPACAL Group Collaboration], Nucl. Instrum. Meth. A **374** (1996) 149.
- [21] K. Hagiwara *et al.* [Particle Data Group], Phys. Rev. D **66** (2002) 010001.
- [22] R. Brun, F. Bruyant, M. Maire, A. C. McPherson and P. Zancarini, CERN-DD/EE/84-1.
- [23] L.R. West, *Talk presented at “Workshop on Monte Carlo Generators for HERA Physics”, Hamburg, Germany, 27-30 Apr 1998*  
(available from <http://www.desy.de/~heramc/mclist.html>)
- [24] M. Gluck, E. Reya and A. Vogt, Z. Phys. C **67** (1995) 433.
- [25] T. Sjöstrand, Comput. Phys. Commun. **82** (1994) 74.
- [26] B. List and A. Mastroberardino, *Prepared for “Workshop on Monte Carlo Generators for HERA Physics”, Hamburg, Germany, 27-30 Apr 1998.*
- [27] S. P. Baranov, O. Dünger, H. Shooshtari and J. A. M. Vermaseren, “LPAIR: A generator for lepton pair production”, In “Hamburg 1991, Proceedings, Physics at HERA, vol. 3” 1478-1482. (see HIGH ENERGY PHYSICS INDEX 30 (1992) No. 12988).
- [28] V. M. Budnev, I. F. Ginzburg, G. V. Meledin and V. G. Serbo, Phys. Rept. **15** (1974) 181.
- [29] C. Adloff *et al.* [H1 Collaboration], Phys. Lett. B **483** (2000) 23 [hep-ex/0003020].
- [30] S. Chekanov *et al.* [ZEUS Collaboration], Eur. Phys. J. C **24** (2002) 345 [hep-ex/0201043].
- [31] F. Abe *et al.* [CDF Collaboration], Phys. Rev. D **50** (1994) 5518.
- [32] K. Schilling and G. Wolf, Nucl. Phys. B **61** (1973) 381.

| $ t $ range<br>(GeV <sup>2</sup> ) | $\langle  t  \rangle$<br>(GeV <sup>2</sup> ) | $d\sigma/dt$<br>(nb/GeV <sup>2</sup> ) |
|------------------------------------|--|--|
| 2 – 3                              | 2.43   | $5.10 \pm 0.29 \pm 0.65$               |
| 3 – 4                              | 3.45   | $3.08 \pm 0.23 \pm 0.39$               |
| 4 – 5                              | 4.46   | $1.47 \pm 0.15 \pm 0.18$               |
| 5 – 6                              | 5.47   | $0.87 \pm 0.12 \pm 0.11$               |
| 6 – 7                              | 6.47   | $0.610 \pm 0.099 \pm 0.074$            |
| 7 – 9                              | 7.92   | $0.285 \pm 0.046 \pm 0.034$            |
| 9 – 12                             | 10.4   | $0.151 \pm 0.026 \pm 0.017$            |
| 12 – 15                            | 13.4   | $0.093 \pm 0.020 \pm 0.010$            |
| 15 – 21                            | 17.7   | $0.0236 \pm 0.0067 \pm 0.0027$         |
| 21 – 30                            | 25.0   | $0.0045 \pm 0.0023 \pm 0.0005$         |

Table 1: The differential photoproduction cross section  $d\sigma/dt$  in the kinematic range  $50 < W_{\gamma p} < 150$  GeV and  $z > 0.95$ . The first uncertainty is statistical and the second is systematic.

| $W_{\gamma p}$ range<br>(GeV) | $\langle W_{\gamma p} \rangle$<br>(GeV) | $\sigma_{\gamma p}$<br>(nb) |
|-------------------------------|---|-----------------------------|
| 50 – 68                       | 58.4                                    | $7.26 \pm 0.57 \pm 0.85$    |
| 68 – 86                       | 76.5                                    | $8.11 \pm 0.68 \pm 0.90$    |
| 86 – 104                      | 94.6                                    | $9.22 \pm 0.87 \pm 1.06$    |
| 104 – 122                     | 113                                     | $13.5 \pm 1.4 \pm 1.7$      |
| 122 – 140                     | 131                                     | $13.0 \pm 1.8 \pm 1.9$      |
| 140 – 160                     | 150                                     | $14.0 \pm 2.2 \pm 2.4$      |

Table 2: The photoproduction cross section as a function of  $W_{\gamma p}$  integrated over the kinematic range  $2 < |t| < 5$  GeV<sup>2</sup> and  $z > 0.95$ . The first uncertainty is statistical and the second is systematic.

| $W_{\gamma p}$ range<br>(GeV) | $\langle W_{\gamma p} \rangle$<br>(GeV) | $\sigma_{\gamma p}$<br>(nb) |
|-------------------------------|---|-----------------------------|
| 50 – 82.5                     | 64.4                                    | $1.24 \pm 0.18 \pm 0.14$    |
| 82.5 – 115                    | 97.4                                    | $2.75 \pm 0.35 \pm 0.31$    |
| 115 – 147.5                   | 130                                     | $3.98 \pm 0.69 \pm 0.57$    |
| 147.5 – 180                   | 163                                     | $3.26 \pm 0.98 \pm 0.58$    |

Table 3: The photoproduction cross section as a function of  $W_{\gamma p}$  integrated over the kinematic range  $5 < |t| < 10$  GeV<sup>2</sup> and  $z > 0.95$ . The first uncertainty is statistical and the second is systematic.

| $W_{\gamma p}$ range<br>(GeV) | $\langle W_{\gamma p} \rangle$<br>(GeV) | $\sigma_{\gamma p}$<br>(nb) |
|-------------------------------|---|-----------------------------|
| 50 – 100                      | 71.0                                    | $0.499 \pm 0.093 \pm 0.060$ |
| 100 – 150                     | 122                                     | $0.94 \pm 0.19 \pm 0.13$    |
| 150 – 200                     | 173                                     | $1.62 \pm 0.52 \pm 0.38$    |

Table 4: The photoproduction cross section as a function of  $W_{\gamma p}$  integrated over the kinematic range  $10 < |t| < 30 \text{ GeV}^2$  and  $z > 0.95$ . The first uncertainty is statistical and the second is systematic.

| $ t $ range<br>(GeV <sup>2</sup> ) | $\langle  t  \rangle$<br>(GeV <sup>2</sup> ) | $\delta$                 | $\alpha$                    |
|------------------------------------|--|--------------------------|-----------------------------|
| 2 – 5                              | 3.06   | $0.77 \pm 0.14 \pm 0.10$ | $1.193 \pm 0.035 \pm 0.025$ |
| 5 – 10                             | 6.93   | $1.29 \pm 0.23 \pm 0.16$ | $1.322 \pm 0.057 \pm 0.040$ |
| 10 – 30                            | 16.5   | $1.28 \pm 0.39 \pm 0.36$ | $1.322 \pm 0.097 \pm 0.090$ |

Table 5: The value of  $\delta$  obtained when applying a fit to the data of the form  $\sigma(W_{\gamma p}) \propto W_{\gamma p}^\delta$  for each  $|t|$  range, together with the corresponding value of  $\alpha$  obtained from  $\alpha = (\delta + 4)/4$ . The first uncertainty is statistical and the second is systematic.

| $\langle  t  \rangle$<br>(GeV <sup>2</sup> ) | $r_{1-1}^{04}$               | $r_{00}^{04}$             | $\text{Re}\{r_{10}^{04}\}$  |
|--|------------------------------|---------------------------|-----------------------------|
| 3.06   | $-0.047 \pm 0.067 \pm 0.009$ | $0.01 \pm 0.12 \pm 0.04$  | $0.022 \pm 0.069 \pm 0.035$ |
| 6.93   | $-0.07 \pm 0.14 \pm 0.07$    | $-0.03 \pm 0.17 \pm 0.02$ | $0.06 \pm 0.12 \pm 0.05$    |
| 16.5   | $-0.19 \pm 0.22 \pm 0.12$    | $0.04 \pm 0.28 \pm 0.04$  | $-0.08 \pm 0.19 \pm 0.08$   |

Table 6: The spin density matrix elements for the kinematic range  $50 < W_{\gamma p} < 150 \text{ GeV}$  and  $z > 0.95$ . The first uncertainty is statistical and the second is systematic. The data are quoted at the average  $|t|$  values over the ranges given in table 5.

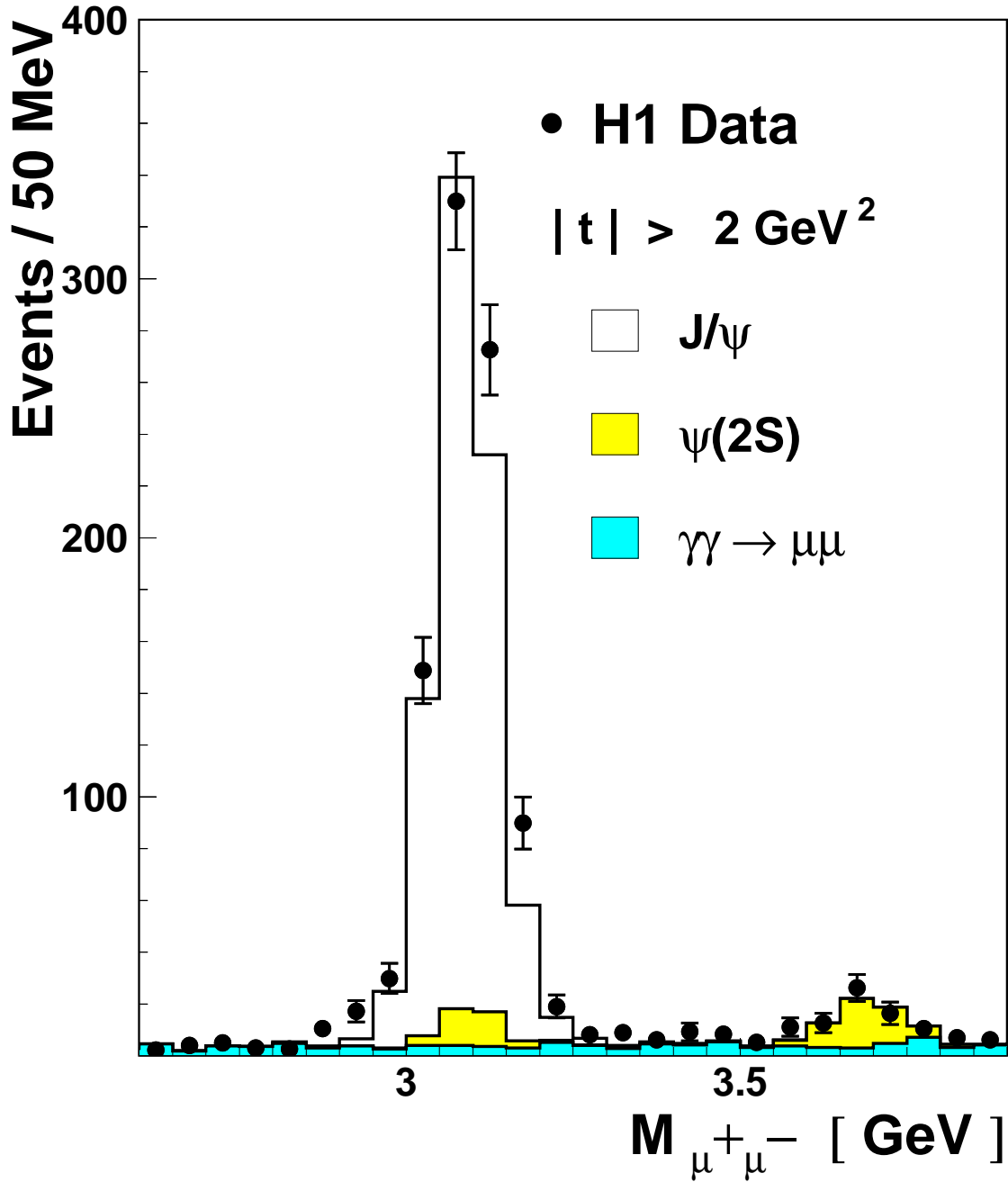


Figure 1: The  $\mu^+\mu^-$  invariant mass distribution in the kinematic region  $50 < W_{\gamma p} < 150 \text{ GeV}$ ,  $z > 0.95$  and  $|t| > 2 \text{ GeV}^2$ . The histogram shows the sum of the Monte Carlo simulations of  $J/\psi$  production using HITVM (open histogram), the contribution from lepton pair production as simulated by the LPAIR program (dark shaded histogram) and the contribution from diffractive  $\psi(2S)$  events as simulated with the DIFFVM program (light shaded histogram).

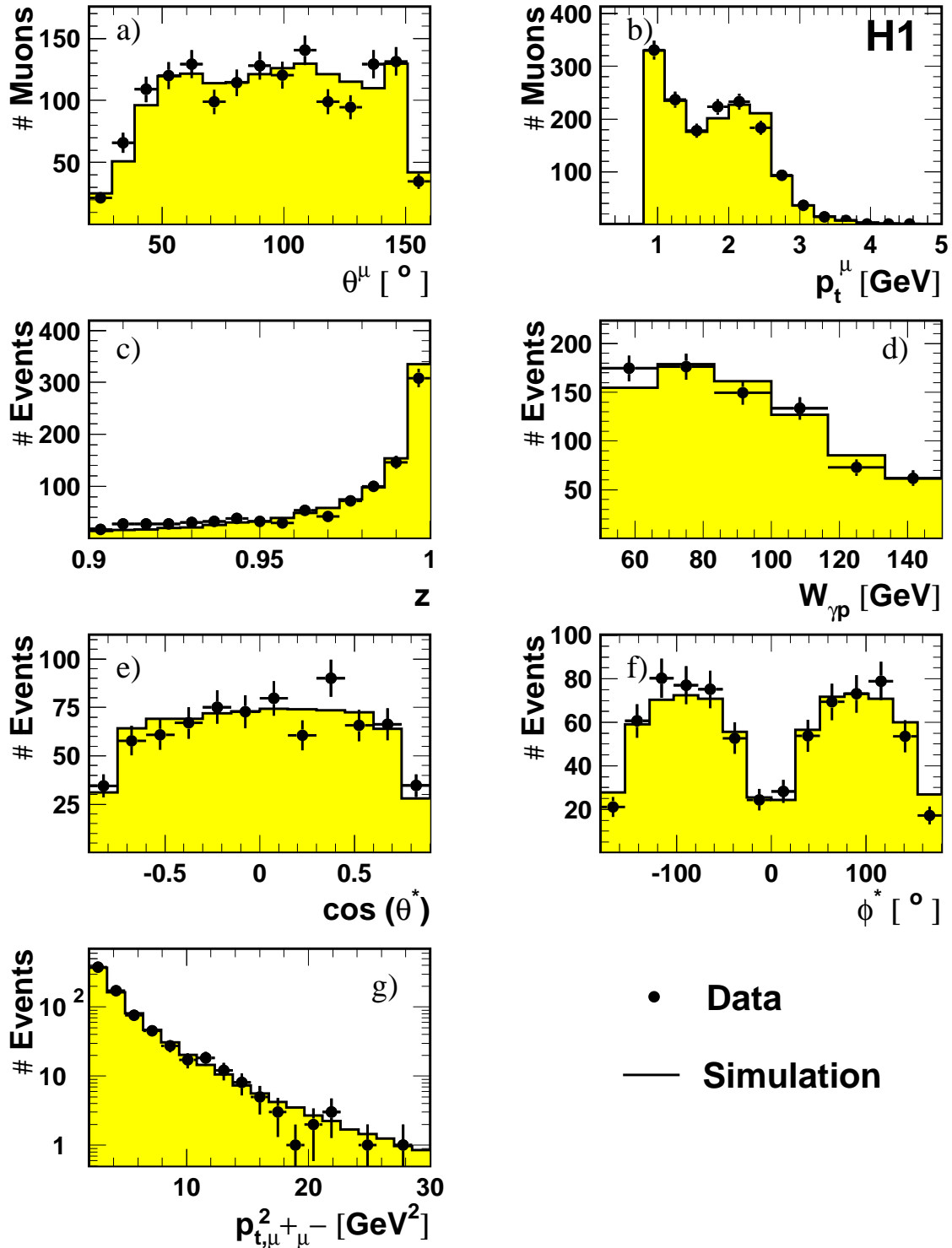


Figure 2: Kinematic distributions of the dimuon sample in the mass range  $2.9 < M_{\mu^+\mu^-} < 3.3$  GeV. a) The polar angle  $\theta^\mu$  and b) the transverse momentum  $p_t^\mu$  of the muon tracks. c) The elasticity  $z$  and d) the photon-proton centre-of-mass energy  $W_{\gamma p}$ . e) The distribution of the cosine of the polar angle and f) the azimuthal distribution of the positively charged decay muon in the helicity frame. g) The distribution of the squared dimuon transverse momentum.

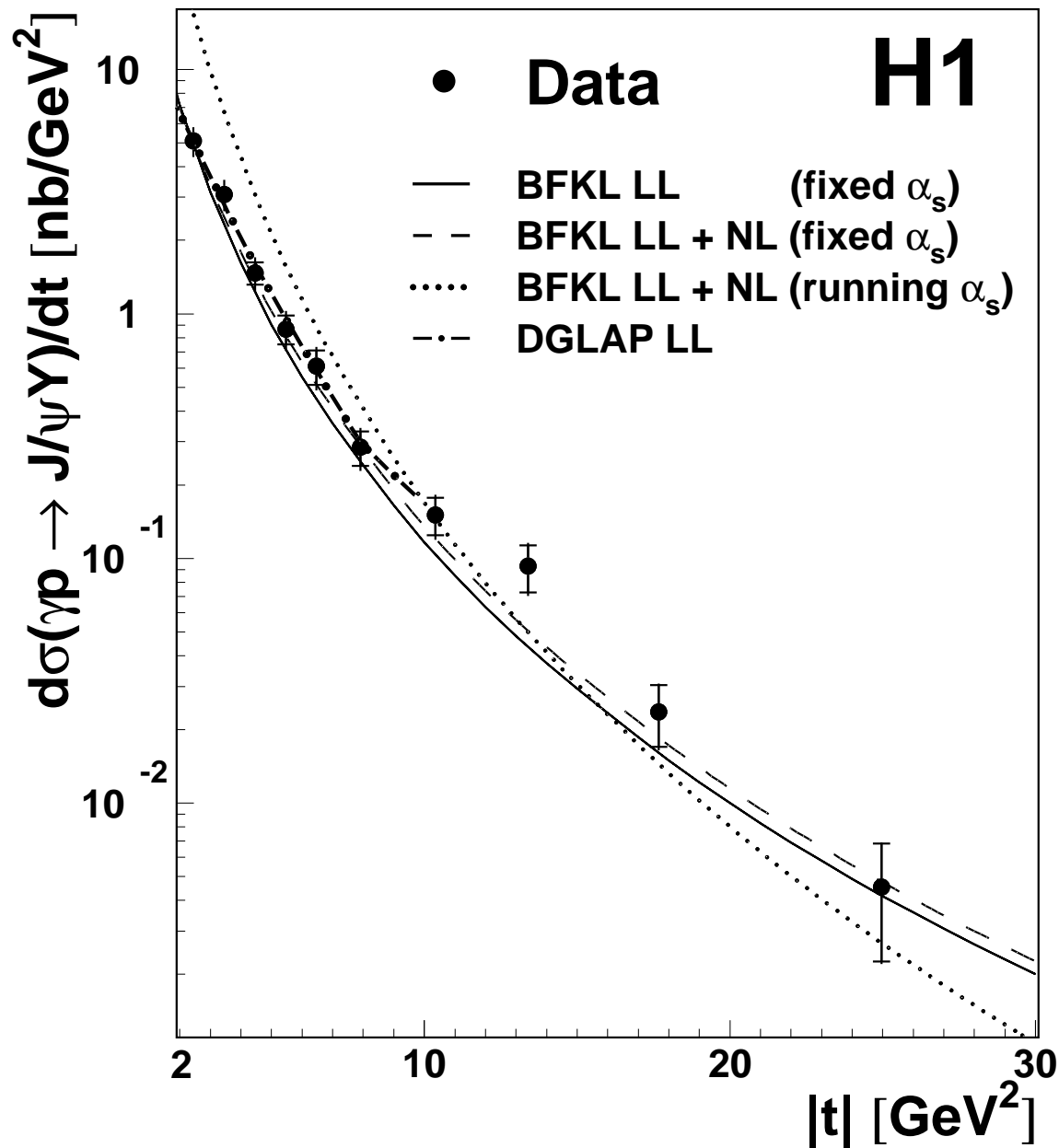


Figure 3: The photon-proton differential cross section  $d\sigma/dt$  for  $J/\psi$  production in the kinematic range  $50 < W_{\gamma p} < 150$  GeV,  $|t| > 2.0$  GeV<sup>2</sup> and  $z > 0.95$ . The inner error bars correspond to the statistical error and the outer error bars are the statistical and systematic errors added in quadrature. The solid line shows the prediction from the BFKL calculation in the leading logarithmic approximation for fixed  $\alpha_s$  [15]. The dashed (dotted) curve corresponds to the BFKL calculation including non-leading corrections and using a fixed (running)  $\alpha_s$  [15]. The dashed-dotted curve, shown in the range  $|t| < M_{J/\psi}^2$ , shows a calculation based on the DGLAP equation in the leading logarithmic approximation [13].

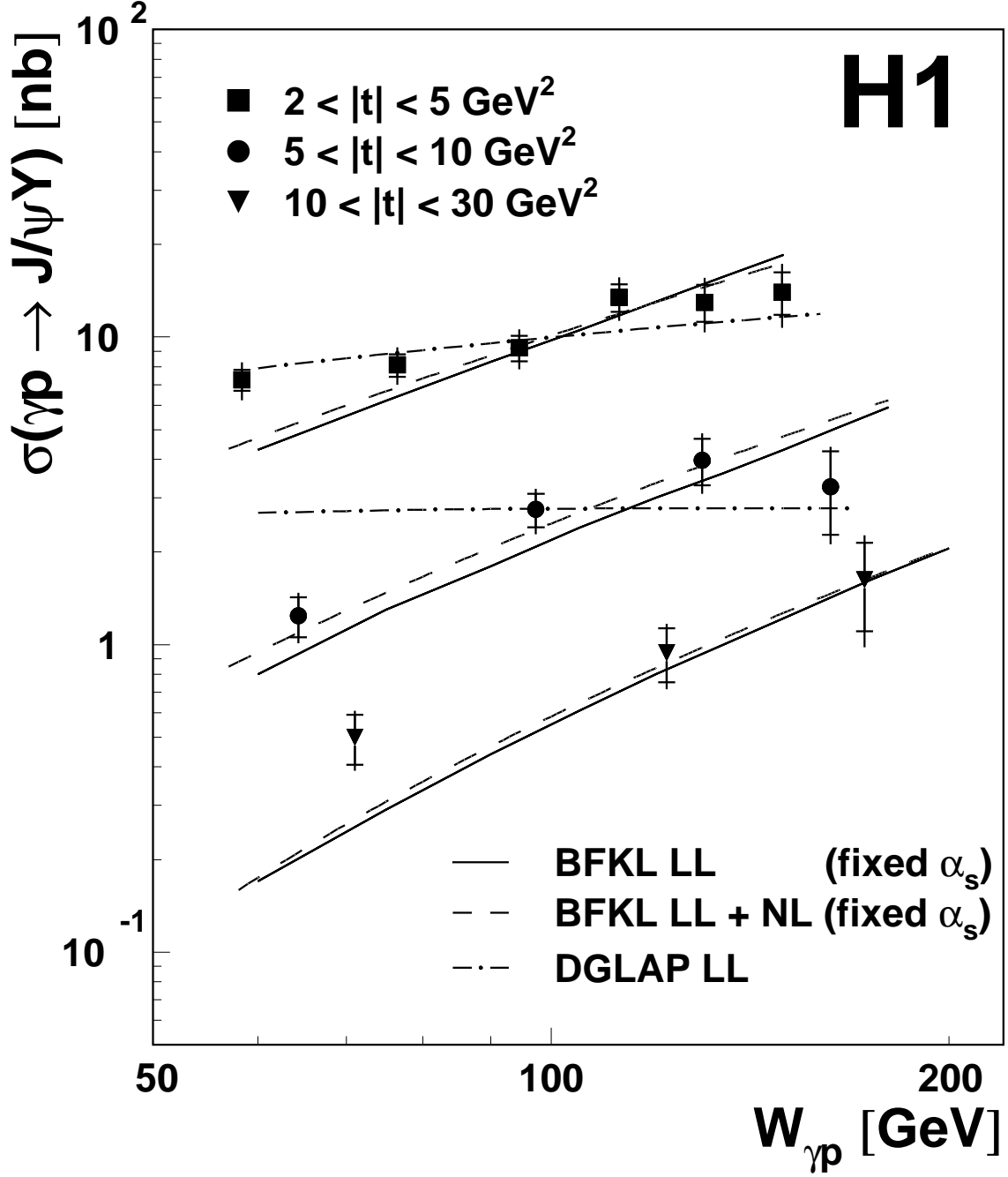


Figure 4: The photon-proton cross section as a function of  $W_{\gamma p}$  in three bins of  $|t|$ . The inner error bars correspond to the statistical error and the outer error bars are the statistical and systematic errors added in quadrature. The solid lines show the predictions from the BFKL calculation in the leading logarithmic approximation and the dashed lines correspond to the BFKL calculation including non-leading corrections using a fixed  $\alpha_s$  [15]. The dashed-dotted curve is the result of a calculation based on the DGLAP equation in the leading logarithmic approximation [13].

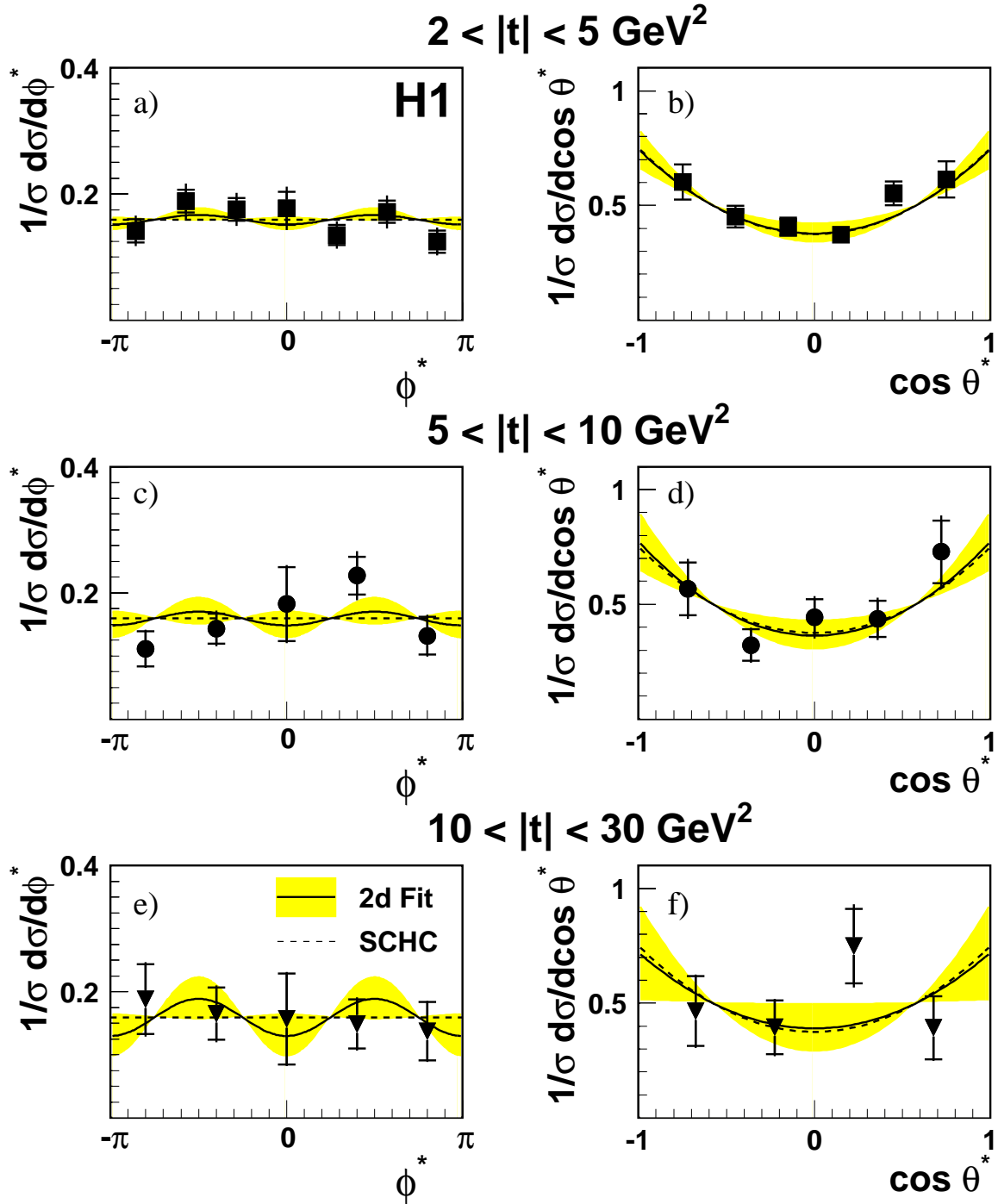


Figure 5: Normalised decay angular distributions for  $J/\psi$  meson production in three bins of  $|t|$ : a,b)  $2 < |t| < 5 \text{ GeV}^2$ ; c,d)  $5 < |t| < 10 \text{ GeV}^2$  and e,f)  $10 < |t| < 30 \text{ GeV}^2$ . The left column (a,c,e) shows the azimuthal distributions of the positively charged decay muon in the helicity frame and the right column (b,d,f) shows the polar angle distributions. The inner error bars show the statistical error and the outer error bars show the statistical and systematic errors added in quadrature. The solid lines show the results of a two-dimensional fit to the data (see text). The shaded band represents the statistical uncertainty for the fit. The dashed line shows the expectation from  $s$ -channel helicity conservation.

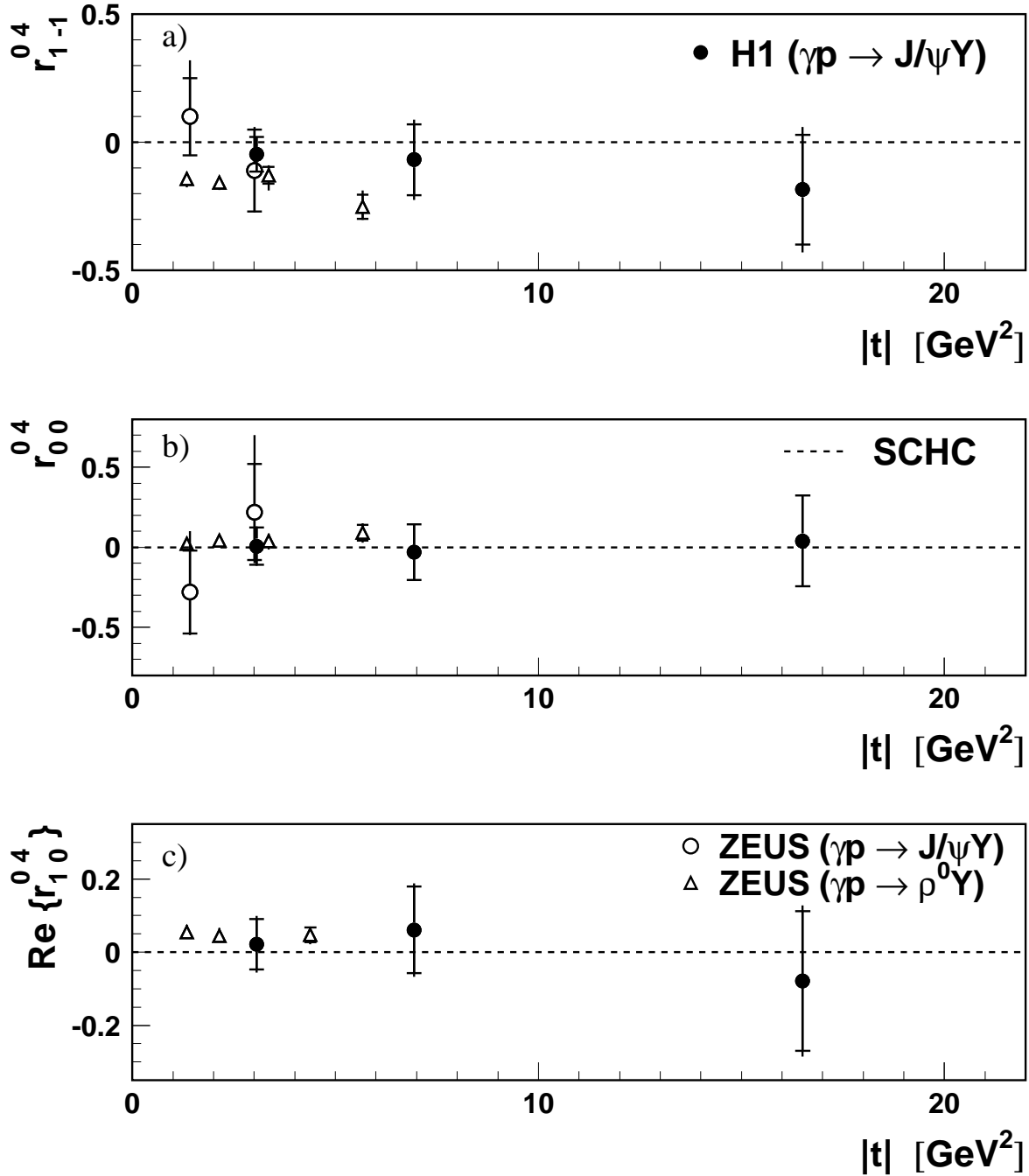


Figure 6: The three spin density matrix elements a)  $r_{1-1}^{04}$ , b)  $r_{00}^{04}$  and c)  $\text{Re}\{r_{10}^{04}\}$  for the  $J/\psi$  as a function of  $|t|$ . The inner error bars represent the statistical uncertainty and the outer error bars the combined statistical and systematic uncertainties. The dashed line shows the expectation from SCHC. The results from the ZEUS collaboration for the photoproduction of  $J/\psi$  and  $\rho^0$  mesons [14] are also shown.